Received: 4 November 2021 | Revised: 17 February 2022 | Accepted: 4 March 2022

High Voltage

DOI: 10.1049/hve2.12212

ORIGINAL RESEARCH

Investigation on effect of semiconducting screen on space charge behaviour of polypropylene-based polymers for HVDC cables

Mingyu Zhou[1] | **Haitian Wang**[1] | **Xintong Ren**[2] | **George Chen**[2] | **Yi Luo**[1] | **Fan Yu**[3]

[1]Global Energy Interconnection Research Institute Europe GmbH, Berlin, Germany

[2]The Tony Davies High Voltage Laboratory, University of Southampton, Southampton, Hampshire, UK

[3]Global Energy Interconnection Research Institute Co., Ltd., Beijing, China

Correspondence

Xintong Ren, The Tony Davis High Voltage Laboratory, University of Southampton, SO17 1BJ Southampton, Hampshire, UK.
Email: Xintong.Ren@soton.ac.uk

Associate Editor: Yasuhiro Tanaka

Funding information

Science and Technology Project of SGCC, Grant/Award Number: 5500-201958504A-0-0-00

Abstract

High voltage direct current (HVDC) power transmission cable is critical for realising sustainability through renewable energy revolution. Eco-friendly thermoplastic polypropylene (PP)-based polymers/nanocomposites are regarded as promising candidates for replacing current thermoset crosslinked polyethylene (XLPE) cables. As an essential component of the extruded HVDC cable for improving conductor/insulation interface and suppressing charge injection to insulation at high DC electrical stresses, developing semiconducting (SC) screens that are compatible with PP-based insulation is of similar importance but has not been well studied yet. This work aims at designing PP-based semiconducting screens and investigating space charge behaviours of SC/PP/SC sandwich specimen to unfold the effect of semiconducting materials, bonding methods, applied DC electric field, and temperature on charge injection, accumulation, transportation, and dissipation in PP-based insulation. Although conventional thermal, mechanical, and low field electrical characterisations demonstrated that all of the developed semiconducting materials meet the performance criteria of commercial semiconducting materials, their space charge and local electric field distribution varied significantly at high DC fields. Compared with the traditional non-bonded configuration used at lab-scale, charge injection was enhanced in hot-pressed SC/PP/SC samples with tightly bonded interfaces, which better reflects the real situation in extruded cables. High temperature further intensified charge injections. Besides, our results also revealed that high temperature and electric field strongly influence charge mobilities and consequently their distribution and local electric field in PP-based insulations.

1 | INTRODUCTION

High voltage direct current (HVDC) power transmission technology is highly desirable for supporting the expeditious development of renewable energy resources and power plants owing to its capability of coping with power fluctuations, lower energy loss during long distance transmission, and high controllability compared with high voltage alternative current (HVAC) technology [1–3]. Developing low-cost, eco-friendly, and highly reliable HVDC power transmission cable is one of the biggest challenges. Among currently available HVDC cables (*e.g.*, mass-impregnated nondraining (MIND) cable, oil-filled (OF) cable, polypropylene laminated paper (PPLP) cable, extruded polymeric insulation cable, etc.), extrudable polymer-based cable outperforms in terms of its high operation temperature, low installation and maintenance cost, eliminated risk of oil leakage, chemical and mechanical stability [4–7]. Extruded polymeric cable with coaxial structure is composed of metal conductor, conductor screen (inner semiconducting screen), insulation, insulation screen (outer semiconducting

Mingyu Zhou and Xintong Ren equal contributions to this work.

screen), metal sheath, and jacket from inner to outer layer [1]. Although the performance and voltage rating of the HVDC cable mainly relies on the properties of insulation, the critical role played by the semiconducting screen in improving the interfacial compatibility between the metal conductor and polymer insulation as well as suppressing charge injection for ensuring safety operation and long-term service of cables shall not be overlooked [8–12].

Typical semiconducting screens are conductive polymer composites that are made of similar base polymer as the insulation and conductive particles [12–14]. As crosslinked polyethylene (XLPE) is one of most widely used insulating polymers for HVAC cables and could be modified for HVDC cables, most of the previous research on semiconducting screen development also centred on XLPE-based materials. According to the reported works and IEC standards (IEC 60840:2020; IEC 60811-501:2012), a well-qualified semiconducting screen should fulfil the following requirements: (1) outstanding processability for extrusion and compatibility with the insulation; (2) high surface smoothness (surface protrusion <125 μm) for reducing interfacial defects between the insulation and semiconducting screen; (3) low volume electrical resistivity (<100 Ω · cm at 25°C; <1000 Ω · cm at 90°C); (4) mechanical robustness with high flexibility, strength, and toughness; (5) stable electrical and mechanical properties over a broad temperature range (−45–90°C) [15, 16].

To achieve all these desirable properties, raw chemicals (*e.g.*, base polymer, conductive filler, antioxidant, *etc.*) and processing methods should be carefully selected and designed. Nilsson et al. reported that heterocharges accumulation near the cathode was greatly suppressed and local electric field distortion was reduced from 78% to 3% via replacing the polar Ethylene butyl acrylate (EBA) matrix with non-polar low-density polyethylene (LDPE) or low-pressure polyethylene (LPPE), suggesting that polar polymers are undesirable for DC applications because low molecular weight polar species in polar polymers might be dissociated by high electric stresses and migrate to the insulation layer to exacerbate charge accumulation [10]. Regarding fillers for constructing conductive networks, carbon black still dominates because of its high dispersibility, low cost, and high conductivity compared with other conductive fillers. The performance of carbon black reinforced semiconducting screens for HVDC cable is controlled by multiple factors, including carbon black type, purity, filler size, concentration, and dispersion state [10, 13, 17–19]. It is widely believed that uniform dispersion of carbon black with high purity and small particle size leads to high electrical conductivity, less space charge accumulation in the insulation interface, and durable mechanical properties. As the developed semiconducting screen is attached to the insulation in practical applications, their compatibility and the interfacial effect should be attentively evaluated as well [8, 11, 20]. According to the experiments and simulation results in Wang et al. and Xiao et al.'s work, local electric fields at semiconducting screen/insulation interface reduced with decreasing particle size of carbon black [20, 21]. Hao et al. demonstrated different bonding methods used for attaching semiconducting screen and insulation also made a difference [11]. Enhanced charge injection from the electrode was found at the interface of tightly bonded semiconducting screen/insulation films compared with conventional sputtered metal electrode/insulation and non-bonded semiconducting screen/insulation films.

Although the well-developed XLPE is still predominant in HVDC cables owing to its superior thermo-mechanical and electrical stability and robustness, one major concern arises from the impurities and by-products introduced during crosslinking, which is considered as the main contribution of space charge accumulation in the XLPE cable. Degassing can effectively remove some of the impurities, but the process requests long-term high-temperature treatment which is time-consuming and costly [22, 23]. More importantly, the thermosetting nature of XLPE makes it nonrecyclable and not sustainable. Recently, recyclable thermoplastic isotactic polypropylene (PP)-based polymers and nanocomposites have been extensively explored for HVDC cable insulations because of their excellent temperature stability, low DC conductivity, and production efficiency [4, 24–27]. Nevertheless, developing PP-based cable insulation still remains at the initial stage due to the rigidity and low fracture toughness. One of the most feasible approaches to address this issue is blending with soft and flexible elastomeric materials, which has been proved effective in improving flexibility and toughness while maintaining good dielectric properties when an appropriate elastomer is employed [28–30]. Compared with the exhaustive research works on PP-based insulations, developing compatible semiconducting materials for PP-based polymers and their combined space charge behaviours have rarely been reported. In this work, three types of PP/elastomer blends-based semiconducting materials were developed and the space charge behaviours of combined semiconducting material/PP were investigated using a pulsed electroacoustic (PEA) system in detail to reveal the effect of semiconducting screen on charge injection, accumulation, migration, and dissipation in PP-based insulations.

2 | EXPERIMENTAL METHODS

2.1 | Materials

Three types of i-PP-based polymers blends were provided by the Global Energy Interconnection Research Institute Co. Ltd (GEIRI) as base polymers for this work, namely PP-A, PP-B, PP-C. PP-A and PP-C are polymer blends (50:50 wt.%) of isotactic polypropylene (i-PP) and propylene-ethylene copolymer (PEC elastomer). Different PEC elastomers were used to prepare PP-A and PP-C. The PEC elastomer in PP-A contains 20–35 wt.% of randomly distributed ethylene. The elastomer and i-PP were supplied by different manufacturers. For the PEC elastomer in PP-C, the content of ethylene is 40–55 wt.% and it is provided by the same manufacture of i-PP. PP-B is a 40:60 wt.% blend of i-PP and blocked copolymer of PP (b-PP). Conductive carbon black pellets (iodine number: 82 mg/g; Oil absorption number (OAN): 190 cc/100g; NSA surface area: 70 m^2/g) with high purity (Ash content: <0.01%; Sulphur

content: <0.02%), Ensaco® 260G, was kindly supplied by Imerys S.A. and was added to base polymers to form conductive networks. A sterically hindered phenolic metal deactivator Irganox® MD 1024 was selected as the primary antioxidant for enhancing both processing and long-term thermal stability of the PP/carbon black nanocomposite as the semiconducting material will be in closely contact with copper conductor during its service life. In addition, a thio-synergic Irganox® PS 802 was used as a secondary antioxidant in combination with the Irganox® MD 1024 to further boost the long-term thermal oxidative stability. Both the Irganox® MD 1024 and the Irganox® PS 802 were kindly provided by the BASF SE.

2.2 | Semiconducting nanocomposites preparation and film fabrication

A melt-blending approach was adopted for preparing PP/carbon black semiconducting composites using HAAKE™ Rheomix QC Lab Mixers (Thermo Fisher Scientific Inc). All base polymers were dried in a vacuum oven at 80°C for 24 h to remove any possible moisture absorbed by the polymer during transportation and storage. PP/carbon black nanocomposites with a weight ratio of 70/30 wt. % were melt-blended at 200°C with a rotation torque of 30 rpm for 20 min to achieve uniform carbon black dispersion in the polymer matrix. 0.1 wt. % of Irganox® MD 1024 and 0.1 wt. % of Irganox® PS 802 were added to the chamber and mixed with the PP/carbon black together. After the mixing process completed, the chamber was opened, and the prepared semiconducting materials were collected for further processing and characterisations.

The collected semiconducting pieces were hot-pressed at 200°C for 5 min using a large press (JBT Engineering) and moulds with various thicknesses for different measurements, followed by cooling in air to room temperature (25°C).

2.3 | Characterisations

Thermogravimetric analysis (TGA) was performed for both pure base polymers and semiconducting materials using a TGA 4000 (Perkin Elmer Inc.) in air atmosphere between 50 and 800°C with a temperature ramp rate of 10°C/min. A scanning electron microscope (SEM), Zeiss EVO 50 XVP (Carl Zeiss AG), was employed to investigate the dispersion of carbon black nanoparticles in base polymers. Cross-sections of the semiconducting screens were obtained by fracturing the films in liquid nitrogen. Gold was sputtered on the sample surface to enhance electrical conductivity. Dumbbell shape semiconducting specimens with thickness of 1.00 ± 0.05 mm were prepared using a sharp puncher for tensile mechanical tests. Specimens were kept at room temperature (25°C) for at least 3 h before testing. Tests were carried out with a Tinius Olsen H25KS Tensiometer (Tinius Olsen) at room temperature (25°C) with a drawing speed of 25 mm/min according to the IEC60811-501 standard. Stress-strain curves were recorded and used for analysing the tensile strength and ultimate elongation of base polymers and semiconducting materials.

Various techniques were employed to investigate electrical properties of the semiconducting samples. Volume electrical resistivity of the semiconducting samples was measured using a 4-probe resistivity measurement system between 25°C and 90°C. Plane samples with size of 5 cm*3 cm and thickness of 100 ± 10 μm was cut from the hot-pressed film and used for tests. The electrical resistance was recorded every 10°C and the volume electrical resistivity was calculated using equation (1) considering the sample geometry and dimensions, where t is the thickness of the sample, V is voltage, and I is current [31].

$$\rho = \frac{\pi}{\ln 2} \cdot t \cdot \frac{V}{I} \tag{1}$$

Space charge profiles of the SC/PP/SC Sandwich film, made of the insulation polymers (PP-A/B/C) bonded with semiconducting materials (SC-A/B/C), were characterised using a PEA system (PEANUT™, Five Lab). As shown in Figure 1, PP and SC were bonded using two different methods, natural gravity pressure from the metal anode (shortened as "natural force" hereafter) and thermal bonding, to form different interfaces between PP and SC for exploring the interfacial effect. Sandwich sample bonded using natural force is a commonly used configuration for measuring space charges under laboratory conditions for its simplicity. However, it is possible to introduce air gaps between the loosely bonded SC/PP interface, resulting in potential acoustic reflection and affecting the accuracy of charge measurement. Meanwhile, the loosely bonded SC/PP interface may hinder charge movement and reduce the charge injection into the polymeric materials, leading to results deviation from practical cable application. Thermally bonded samples were prepared by hot-pressing the stacked SC/PP/SC sandwich film slightly below the melting temperature (T_m) of the base polymer (T_m-5°C) for 5 min to form tightly bonded interfaces and simulate the interface of the triple-extruded cable. Before high DC electric fields (20 kV/mm and 40 kV/mm) were applied, a low DC electric field of 5 kV/mm was applied to the sample for a short period of time (5 s) for calibration and the reference PEA profile was obtained assuming that only capacitive charges were involved and no space charge was injected from the electrodes at this field [32]. High DC field was applied to the sample for 60 min (voltage on) to observe and record the charge injection and accumulation in the PPs during the polarisation process. Charge decay during the depolarisation was subsequently obtained after the sample was short circuited for another 60 min (voltage off). The PEA measurements were performed at both room temperature (25°C) and 60°C to investigate the influence of high temperature on space charge injection and accumulation.

Regarding PEA data processing, to avoid interference of capacitive charges that are overlapped with the space charges and reveal true charge distribution, the reference data obtained at low electric field was used to subtract the surface charges near the electrodes at high field and the normalised voltage-on

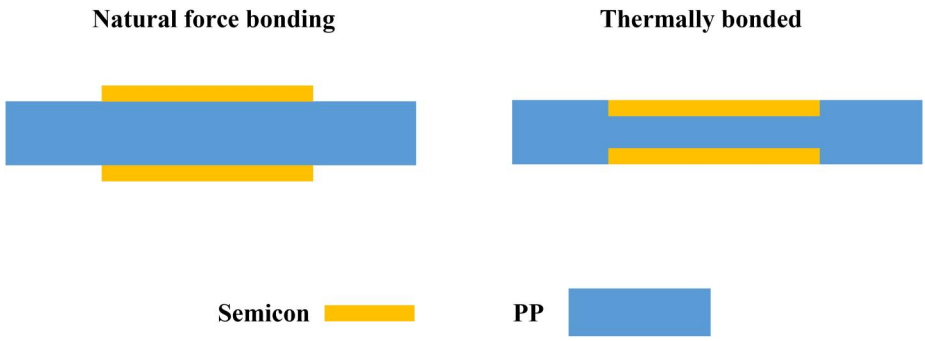

FIGURE 1 Schematic diagrams of SC/PP/SC Sandwich samples for pulsed electroacoustic (PEA) tests

space charge density $\rho_{nor}(x,t)$ was obtained with equation (2) below,

$$\rho_{nor}(x,t) = \rho_{exp}(x,t) - \frac{E_{appl}}{E_{ref}} \cdot \rho_{ref}(x) \quad (2)$$

where x is the distance to the cathode; t is the field application time; $\rho_{ref}(x)$ and $\rho_{exp}(x,t)$ represents the charge density of the reference data and experimentally measured data at point x and time t, respectively; E_{ref} and E_{appl} are the reference and applied electric field, respectively [32, 33]. Local electric field distortion rate was calculated using equation (3),

$$\text{Field distortion rate} = \frac{E_{act} - E_{appl}}{E_{appl}} \times 100\ \% \quad (3)$$

where E_{appl} is the actual electric field obtained from the charge distribution profile.

Considering the fact that various sample thicknesses and slightly different electrode sizes were obtained during sample preparation, average charge density calculated using equation (4) was proposed and was used to evaluate the charge amount in the sample instead of the total charge amount.

$$Q_{ave} = \frac{1}{t \cdot S} \int_0^t \left|\rho_{nor}(x,t)\right| S dx \quad (4)$$

In equation (4), S represents the area of the effective electrode and other parameters are similar to equation (2).

DC conductivity of the SC/PP/SC sandwich films was measured using a home-built system with a fan oven at a DC electric field of 40 kV/mm. The tests were carried out at 25°C and 60°C.

3 | RESULTS AND ANALYSIS

3.1 | Concentration of carbon black and thermal stability of PP-based semiconducting materials

TGA measurements were conducted for both pure base polymers and semiconducting materials to evaluate the actual carbon black concentrations in the semiconducting material and the effectiveness of the antioxidants. As shown in Figure 2a, PP-A demonstrated the highest onset degradation temperature T_{onset} (extrapolated from the TGA curves in Figure 2a) and peak degradation temperature T_p (derived from the first derivative TGA curves in Figure 2b) among the three polymers, suggesting its highest thermal stability at high temperature. The addition of antioxidants into the semiconducting materials improved the thermal stability of these PP-based polymers with remarkably increased T_{onset} and T_p (Figures 2c and 2d, and Table 1) albeit high loading ratios of carbon black could potentially cause severe thermal oxidative degradation at lower temperatures. These results indicate that the selected antioxidants worked effectively for enhancing the thermal stability of the semiconducting materials. The actual concentration of carbon black in the produced semiconducting materials was also validated by the TGA curves in Figure 2c, where 30% of the sample weight remained after heating up to 800°C. This is highly consistent with the expected loading ratios, suggesting no obvious material loss occurred during the melt-blending process.

3.2 | Morphology and surface smoothness of PP-based semiconducting materials

Homogeneous carbon black dispersion in semiconducting materials is highly desirable for achieving high mechanical and electrical properties such as high ultimate elongation strain and low volume electrical resistivity. The dispersion states of carbon black nanoparticles in semiconducting materials are strongly associated with the type and concentration of carbon black as well as processing parameters. The conductivity and dispersibility of carbon black usually contradict with each other. Although superconductive carbon black is helpful for reducing the percolation threshold for building up a conductive network in insulating polymers and alleviating the deterioration of mechanical properties, the difficulty of achieving uniform dispersion is increased. Therefore, a carbon black with balanced conductivity and dispersibility was selected for this work. As shown in the SEM images in Figure 3, all of the three semiconducting films displayed

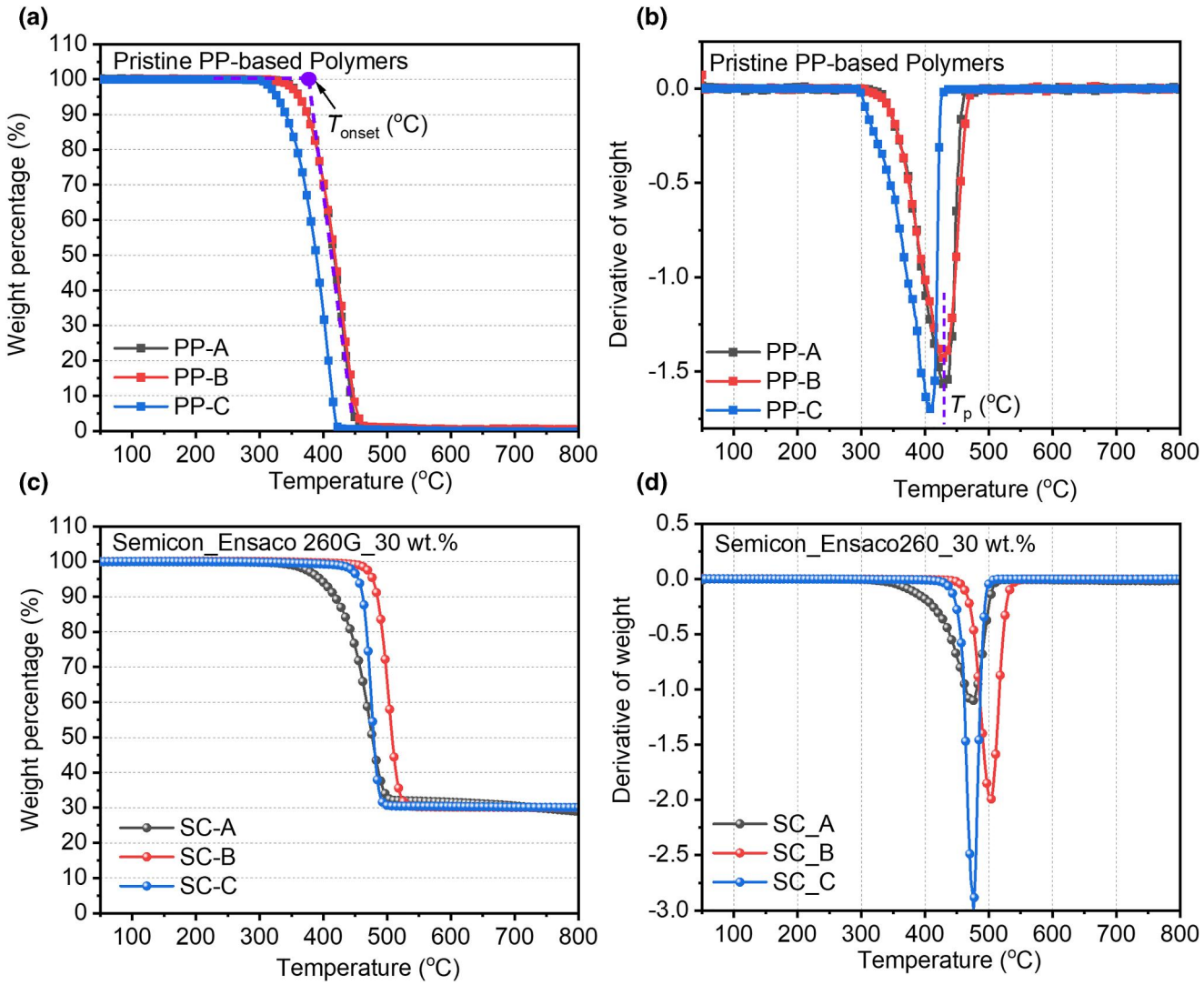

FIGURE 2 (a), (c) Thermogravimetric analysis (TGA) curves and (b), (d) derivative thermogravimetric analysis (DTA) curves of pristine PP-based polymers and semiconducting materials, respectively

TABLE 1 Comparison of onset degradation temperature T_{onset} and peak degradation temperature T_p for pristine PP-based polymers and semiconducting materials

	T_{onset} (°C)		T_P (°C)	
	PP	SC	PP	SC
A	384	421	429	472
B	377	483	427	502
C	359	457	409	475

homogeneous carbon black dispersion in the base polymers as indicated by the bright points in the images. No obvious particle aggregations were found at the cross-sections of the films, suggesting the selected processing conditions are effective for promoting uniform carbon black particle dispersion and leading to desirable mechanical and electrical properties.

3.3 | Mechanical properties of PP-based semiconducting materials

One of the critical limitations that prevents pure i-PP from being used as cable insulation material is the poor flexibility and low mechanical toughness arising from its low glass transition temperature and crystal structure. In the work, elastomers were included into i-PP to improve the mechanical properties of i-PP. As shown in the representative stress-strain curves Figure 4a, all the base polymers are mechanically strong and tough with high ultimate tensile strength and elongation at break. The ultimate strain of PP-B reached 1100%, which is much higher than the reported value for pure i-PP (<50%) without any special treatment. Comparisons of these polymers and prepared semiconducting materials are summarised in Table S1. Although all developed semiconducting materials showed much reduced elongation at break values (Figure 4b) compared with their base polymers due to the high carbon black loading, they still meet the requirement for commercial

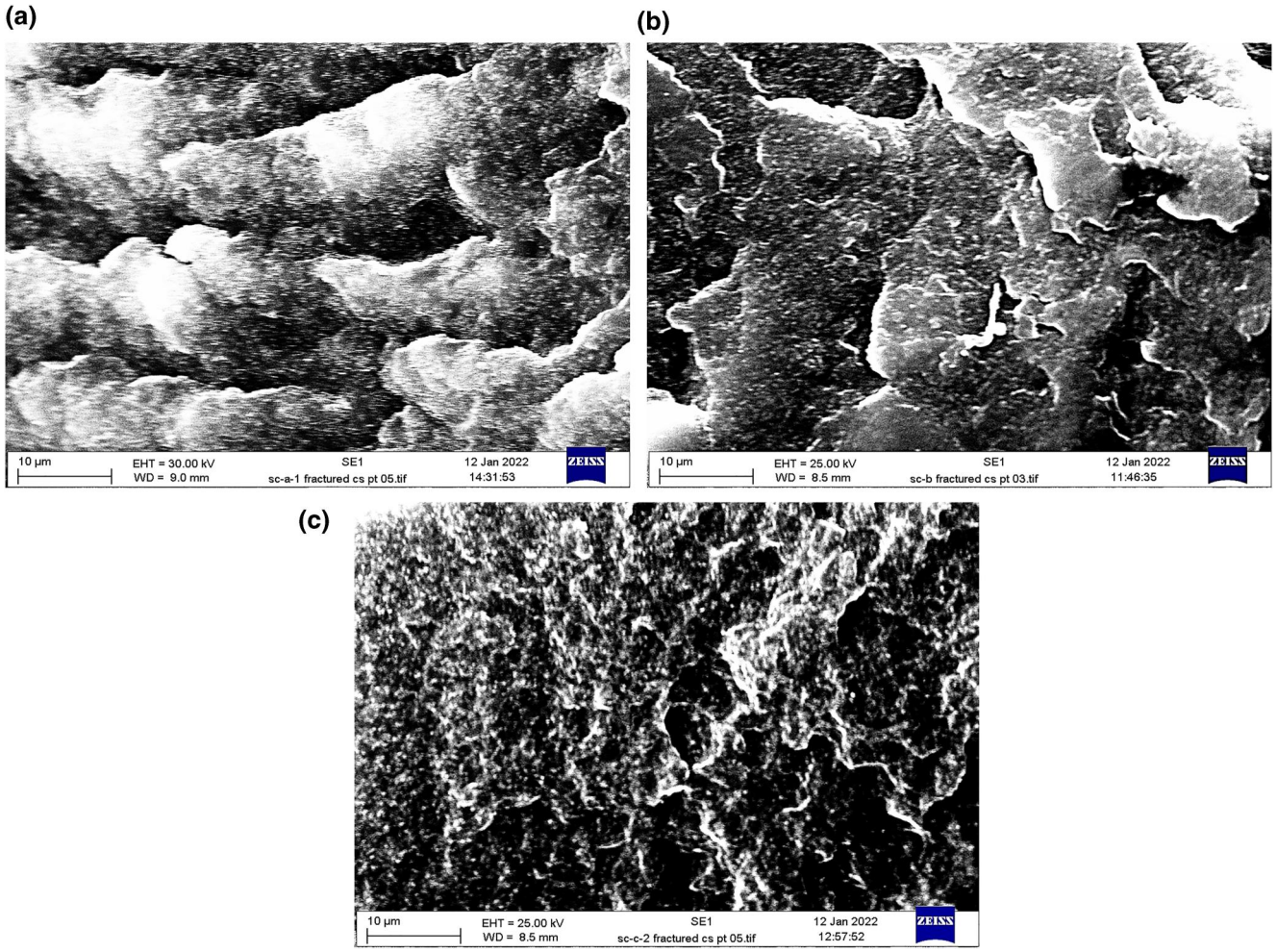

FIGURE 3 Scanning electron microscope images of (a) SC-A; (b) SC-B; (c) SC-C

semiconducting materials (elongation at break >200%, tensile strength >12 MPa), which further confirmed the uniform distribution of carbon black nanoparticles in the base polymers.

3.4 | Volume electrical resistivity of PP-based semiconducting materials

Volume electrical resistivity is another important parameter for evaluating the performance of the semiconducting material, which is directly linked with the loading ratios of carbon black nanoparticles in the polymer matrix and can be explained by the percolation theory. It has been reported that low volume electrical resistivity of the semiconducting screen is beneficial for preventing charge injection and strong local field enhancement near the interface between insulation and semiconducting screen [13]. As presented in Figure 5a, all of the prepared PP-based semiconducting materials exhibited very low volume electric resistivity (<2.1 $\Omega \cdot$ cm), which is nearly 10 times lower than that of a commercial semiconducting material (20.7 $\Omega \cdot$ cm). The outstanding electrical properties of the produced semiconducting materials could be attributed to the thoroughly balanced conductivity and dispersibility of the carbon black, which lead to strong conductive networks.

Generally, volume electrical resistivity of conductive polymer composites tends to increase at high temperatures (known as "positive temperature coefficient" (PTC) effect) due to the high thermal expansion rate of polymer matrix induced disconnected conductive pathway [34, 35]. The increment of the volume electrical resistivity can reach several orders of magnitude when the temperature reaches its melting temperature. As a result, the ability of suppressing charge injected is impaired. And high temperature is inevitable during the cable operation and service because of the Joule heating of the metal conductor. Therefore, it is important to develop semiconducting materials with stable volume electrical resistivity over a broad temperature range. Semiconducting materials prepared in this work using Ensaco® 260G and PP-based polymers displayed relatively small resistivity change at high temperatures up to 90°C (Figure 5b). The highest increase was found in SC-B while the lowest increase was observed in SC-C.

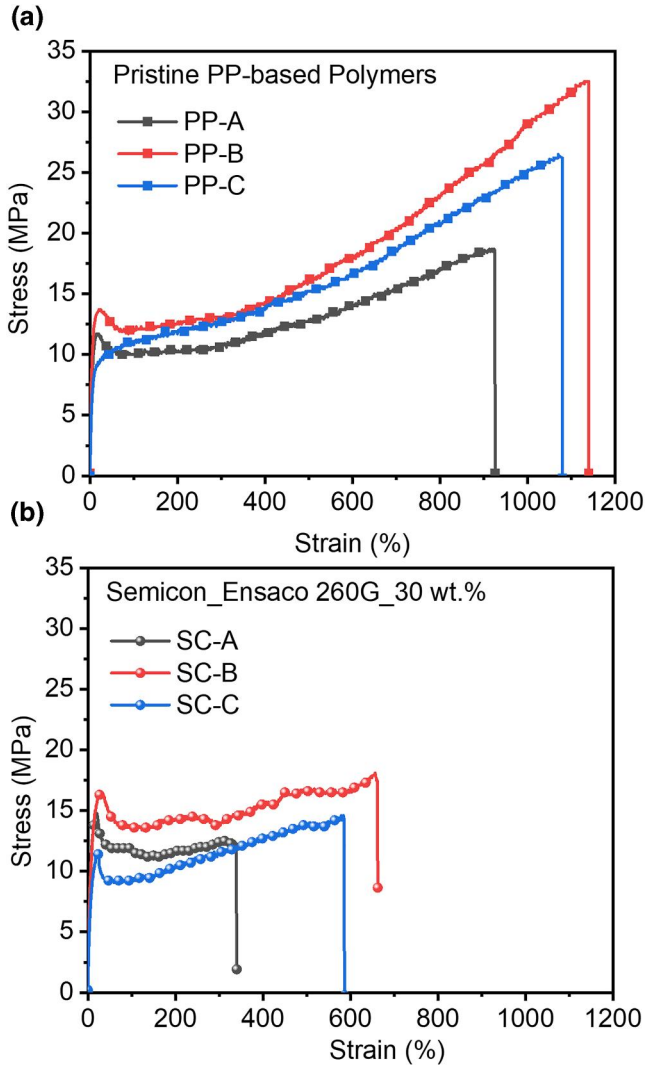

FIGURE 4 Tensile stress-strain curves for (a) pristine PP-based polymers; (b) semiconducting materials

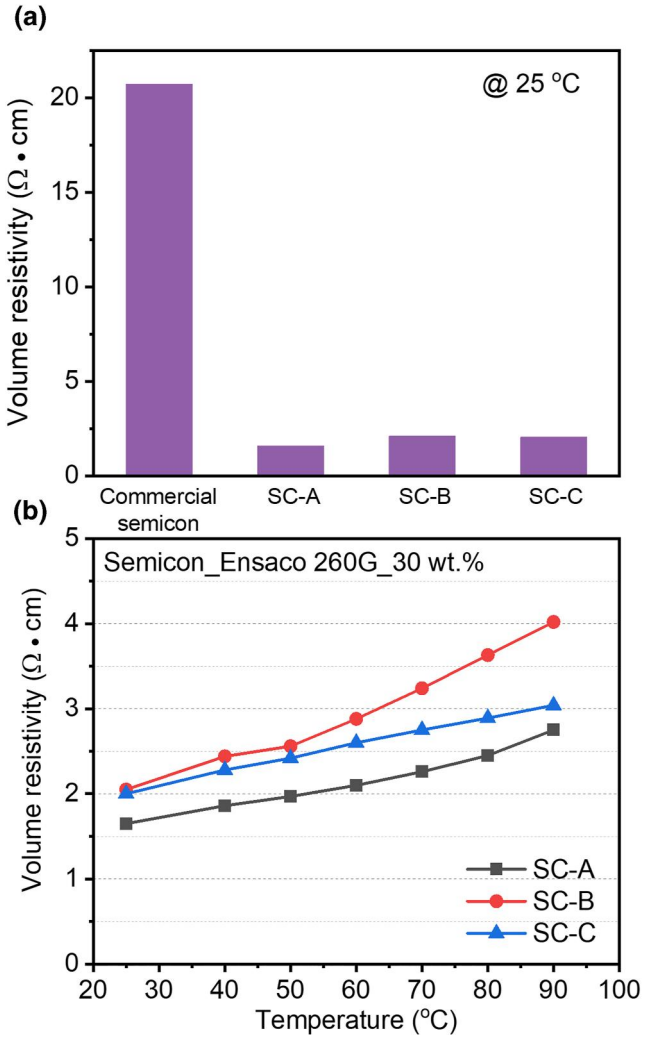

FIGURE 5 Volume electrical resistivity of: (a) SC-A/B/C and a commercial semiconducting material at 25°C; (b) SC-A/B/C as a function of temperature

3.5 | Space charge behaviour of PP-based polymers bonded with semiconducting materials

As discussed before, all prepared semiconducting materials show good mechanical and electrical properties, making them potentially suitable for HVDC cable applications. As semiconducting screens play a critical role in charge injection from the metal conductor to the insulation layer, their performance under high DC fields is highly important. In this section, space charge profiles of PP-based insulating polymers bonded with the prepared semiconducting materials will be investigated. Space charge distribution in insulation materials is sensitive and can be affected by many factors, including semiconducting materials, applied field, temperature, as well as interfacial interaction between the semiconducting layer and the insulating layer [11, 36]. All voltage-on charge distribution profiles shown in the main context are normalised ones to exclude the interference of capacitive charges near the SC/PP interface (referred to section 2.3). Original space charge profiles are presented in the supplemental information (Figure S1–S4) as references.

3.5.1 | Effect of interface between insulation and semiconducting material

To investigate the interfacial effect at SC/PP interface, natural force bonded sandwich samples and thermally bonded samples were prepared according to Figure 1, and PEA measurements were performed. Figure 6 presents normalised space charge distribution and electric field distribution over the thickness of the natural force bonded sandwich samples obtained at 25°C and at DC 40 kV/mm. Heterocharge (positive charges close to the cathode and negative charges close to the anode) accumulations were found near both the cathode (~30 μm) and anode (~190 μm) in PP-A immediately when the DC field was applied (Figure 6a) and no obvious homocharge injection was

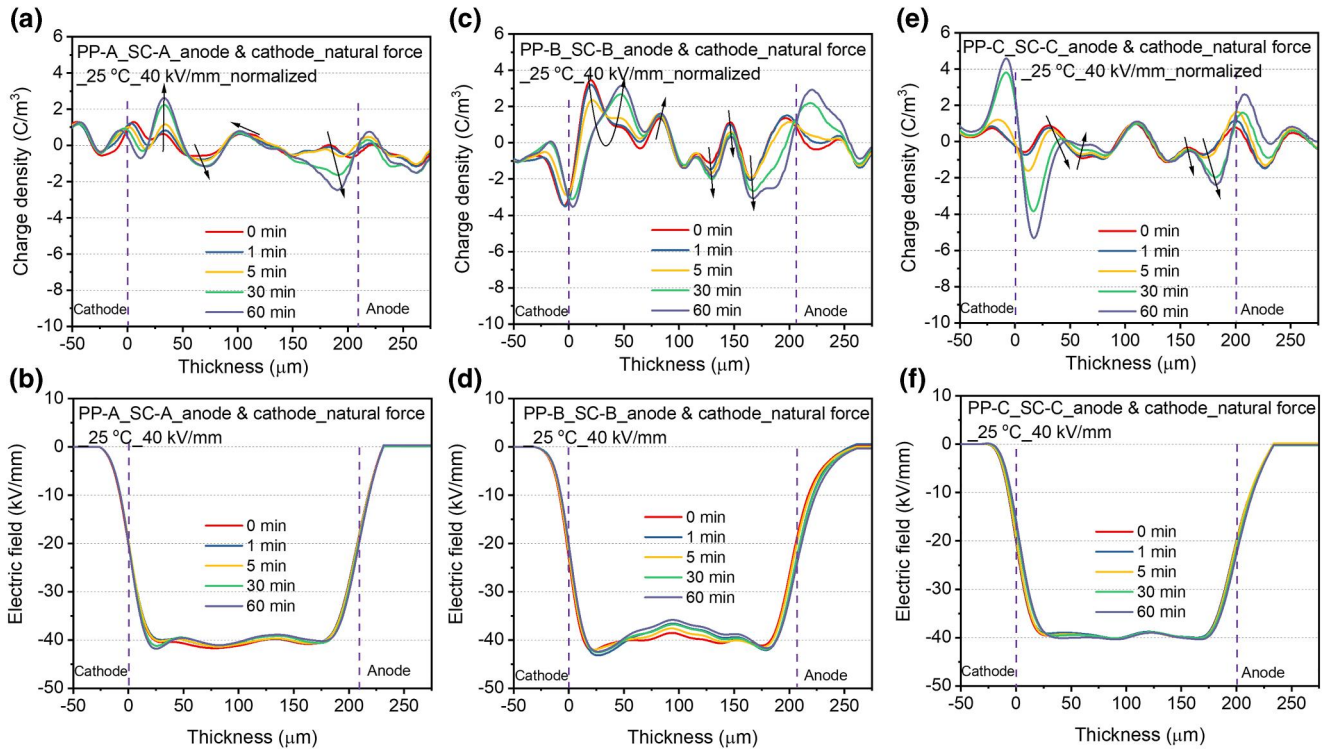

FIGURE 6 Normalised space charge distribution profiles and electric field distortion at DC 40 kV/mm for natural force bonded (a), (b) PP-A; (c), (d) PP-B; (e), (f) PP-C, respectively

observed. The amount of heterocharges increased with time. As a result, the local electric field near the cathode was distorted by 4.3% after applying the DC field for 60 min. During the depolarisation processing shown in Figure S1b, those heterocharges formed during polarisation decreased and saturated after short-circuiting for 20 min. Similar to PP-A, the formation of heterocharges near both the electrodes was also observed in PP-B (Figure 6c) with higher amount of charges compared to PP-A. There are two positive charge peaks near the cathode (25 and 50 μm). On increasing the field application time, the intensity of the positive charge peaks at 25 μm decreased while an enhancement in intensity was observed in the peak at 50 μm. Together with the negative homocharge peak found at the cathode (0 μm), it can be inferred that a stronger homocharge injection happened at the cathode of PP-B than PP-A which recombined with the positive charges and caused the aforementioned peak intensity change. Due to the presence of higher amount of heterocharges, the maximum field distortion rate near the cathode of PP-B reached to 8.1% at 1 min, which reduced to 5.9% after 60 min (Figure 6d) because of charge recombination. The charge distribution profile for PP-C bonded with SC-C using natural force (Figure 6e) is rather different from PP-A and PP-B. At the anode side, a small amount of heterocharges were built up with time, which is similar to PP-A/B. At the cathode side (~30 μm), positive charges (heterocharges) were accumulated from 0 to 5 min. However, these positive charges were gradually neutralised by injected negative charges from cathode and the injected negative homocharges became dominant near the cathode after 20 min. Consequently, the electric field distribution in PP-C is relatively uniform over the insulation thickness with negligible field distortion. Overall, SC/PP/SC samples prepared using natural force bonding showed heterocharge formation near electrodes, which might be associated with the charge accumulation at the interface between i-PP and elastomers and ionisation of impurities. Preliminary trials on different polymers blending systems carried out by the project sponsor revealed that poor cocrystallisation ability and phase separation were found in the PP-B blend. The higher amount of space charge in PP-B also confirms the relative low compatibility between i-PP and block copolymer of PP compared to propylene-ethylene copolymer. Figure 7 displays the PEA results at 40 kV/mm and 25°C for thermally bonded sandwich films. Compared to those samples bonded using natural force, charge injection from metal electrodes was enhanced among thermally bonded samples with tightly coupled interfaces. For the thermally bonded PP-A, homocharge injection near both electrodes were predominant when the DC voltage was applied. The amount of negative homocharges adjacent to the cathode (0–50 μm) increased with time while the positive charges accumulated near the anode (~100–125 μm) decreased with time and finally transformed to negative heterocharges after 40 min. There are two possibilities for this phenomenon. On the one hand, negative charges exhibit higher charge mobility than positive charges. Therefore, the injected negative charges from cathode migrated to anode with increasing time and neutralised with positive charges injected from anode. On the other hand, as the PEA technique

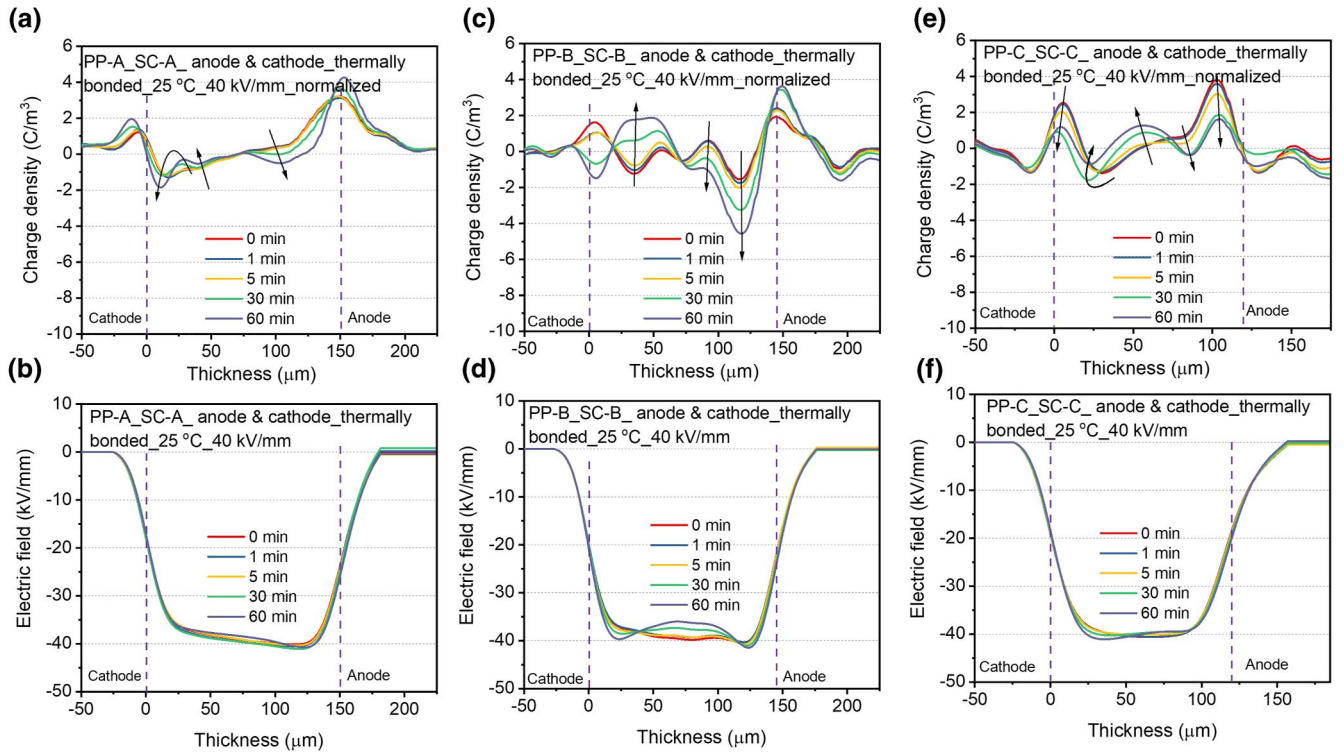

FIGURE 7 Normalised space charge distribution profiles and electric field distortion at DC 40 kV/mm for thermally bonded (a), (b) PP-A; (c), (d) PP-B; (e), (f) PP-C, respectively

measures the net charge, it is possible that the heterocharge formation near the anode is stronger than the homocharge injection from electrode. As a result, the injected positive charges cannot fully compensate the accumulated negative charges and lead to heterocharges build-up near the anode. The competition between the homocharge injection and heterocharge formation was further confirmed by the voltage-off data, where the injected homocharges drifted away quickly after removing the applied field and only heterocharges were left. The maximum field distortion of 1.8% was observed near the anode side due to the presence of heterocharges, which is lower than that of the natural force bonded sample (4.3%).

In the thermally bonded SC-B/PP-B/SC-B sample, the negative homocharge peak was first observed near the cathode and then replaced by the positive heterocharge peak after 20 min (~35 μm) owing to the charge recombination. At the anode side, negative heterocharges were dominant from 0 min and the peak kept increasing with time. Compared with the PP-B bonded with SC-B using natural force, stronger charge injection was observed with a deeper injection thickness near the cathode of the thermally bonded sample. Thanks to the charge recombination near the cathode, the highest field distortion (3.5%, Figure 7d) was seen at the anode.

The thermally bonded SC-C/PP-C/SC-C sample showed a different charge distribution compared with the other two polymers. The injection of positive charges was significantly enhanced with a strong positive peak near the anode. However, the amplitude of this peak decreased, and the peak distribution narrowed with time, suggesting that the injected charges were neutralised by the formed negative heterocharges. A small amount of positive charges appeared in the bulk of the sample, which could have resulted from the combination of the heterocharge formed near the cathode and the homocharge injection from the anode. The electric field distribution in PP-C was relatively flat and uniform.

Instead of the total amount of charge that has been used by other researchers to provide general information on space charge, average charge density (equation (4)) is proposed in this study to investigate the space charge profiles for samples with various dimensions. Results for PP-based polymers with semiconducting materials bonded using natural force and thermally bonded semiconducting materials are presented in Figure 8a (voltage-on) and 8b (voltage-off). Generally, the average charge density increased with time in all the samples using natural force. Among all thermally bonded samples, only PP-B showed the increasing average charge density trend while a decreasing trend was observed in PP-A and PP-C as a result of strong charge recombination between the formed heterocharges and injected homocharges. Compared with propylene-ethylene copolymers in PP-A and PP-C, the blocked copolymer in PP-B contains long non-propylene sequences, which resulted in a relatively lower compatibility with i-PP and resulted in higher amount of space charge accumulation. Regardless of the bonding methods and materials, all samples showed a quick charge dissipation process after short-circuiting and the remained with average charge density reduced below 0.75 C/m^3. Charges in thermally bonded samples SC-B/PP-B/SC-B and SC-C/PP-C/SC-C drifted away with a slower speed

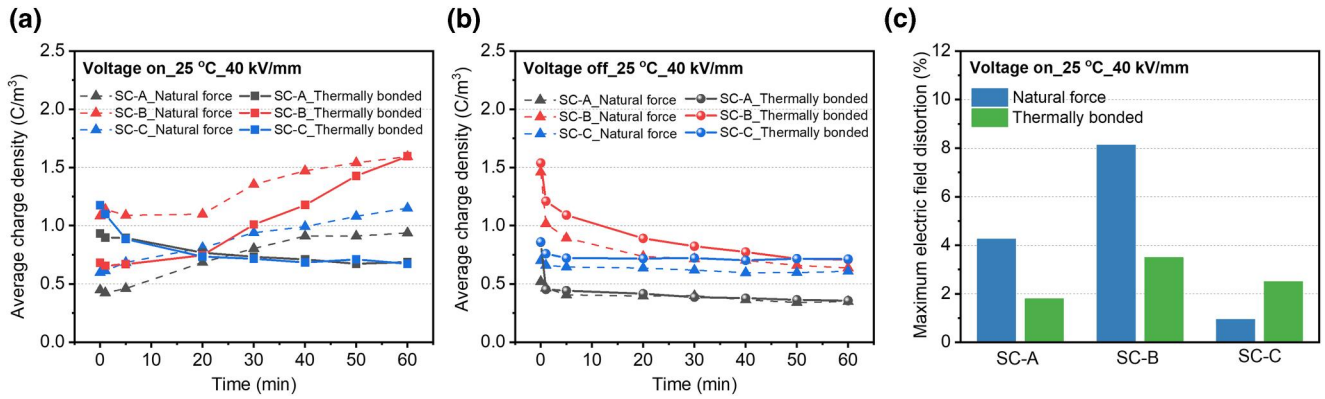

FIGURE 8 Average charge density of PP-based polymers bonded with the prepared semiconducting materials using different bonding methods during (a) voltage-on (DC 40 kV/mm); (b) voltage off. (c) Maximum field distortion observed during the voltage-on process of PP-based polymers bonded with the prepared semiconducting materials

compared with samples prepared using natural force, which can be ascribed to the tightly bonded semiconducting/insulating interface.

The maximum field distortion values for all samples are summarised and presented in Figure 8c. Apparently, PP-B exhibited the highest local electric field enhancement due to the highest amount of heterocharges. Thermal bonding not only dramatically facilitated the charge injection from electrodes but also changed the charge distribution in PP-A/C. They exhibited different field distortion enhancements although both of them showed similar decreasing trend with close average charge density values. A stronger negative charge injection was found in PP-A while a stronger positive charge injection was dominant in PP-C, leading to different results.

3.5.2 | Effect of temperature and electric field

The effect of temperature on space charge distribution of thermally bonded sandwich samples was explored via performing PEA measurement at 60°C. As analysed in the previous section, thermal bonding facilitated the charge injection at both electrodes and neutralised the heterocharges in PP-A, leading to suppressed electric field distortion at the semiconducting material/insulation interface. However, when the SC-A/PP-A/SC-A sample was subjected to a DC field of 20 kV/mm at 60°C, negative heterocharges appeared at the anode side again (Figure 9a). Two possible reasons are considered to account for this phenomenon. One is the greatly enhanced negative charge mobility at high temperature, which renders the injected negative charges at the cathode ability to migrate to the anode and accumulate there. The other possibility is that the positive charges injected from the anode with high mobility quickly transported from the electrode to the middle of the sample and recombined with the injected negative charges from the cathode, leaving behind the heterocharges formed at the anode side. Adjacent to the injected negative charge peak (~10 μm), a positive heterocharge peak was observed, which could be ascribed to similar reasons as the heterocharge peak at the anode. As a result of the heterocharges at both electrodes, the local electric field was distorted with the maximum value of 9.9% found at the cathode (Figure 9b).

Compared with PP-A, high temperature has a more severe impact on PP-B and resulted in a huge field distortion value of 55.0% near the cathode at 1 min (Figure 9d). As shown in Figures 9c, a large amount of positive charges accumulated next to the negative charge peak at the cathode as well as the middle of the sample. This broad positive charge peak kept shifting to the anode side and the amplitude of the peak decreased with time, which could be attributed to the charge recombination that happened between the injected negative charges and the positive charges in the middle of the sample. When the DC field was removed, homocharges were found at both the cathode and the anode (Figure S3d). The positive charges at the anode quickly drifted away while the negative charges at the cathode slowly dissipated with time. The amount of positive charges in the bulk sample observed during the polarisation process also decreased with a small amount of them remaining in the sample after 60 min.

As for PP-C, positive space charge accumulation was obvious and dominant in the original voltage-on PEA profile (Figure S3e). Removing the capacitive charges produced a clearer charge distribution profile in Figure 9e. This is consistent with the data at 25°C where positive charge injection from the anode was remarkably enhanced by the thermal bonding. And the mobility of these charges was enhanced by the high temperature. Therefore, positive charges were evenly distributed in the middle of the sample (30–105 μm). The highest field distortion was located near the cathode (13.0%, Figure 9f) because of the existence of positive heterocharges.

Increasing the DC electric field to 40 kV/mm gave rise to higher charge mobility than at 20 kV/mm. The normalised voltage-on charge distribution and corresponding electric field distortion results are shown in Figure 10. For PP-A, negative charges were dominant in the bulk sample when the electric field was just applied at 0 min. The negative charges near the cathode were replaced by positive charges after 1 min (25–60 μm); The injected negative charge peak at the cathode and the positive heterocharge peak next to it constantly shifted to

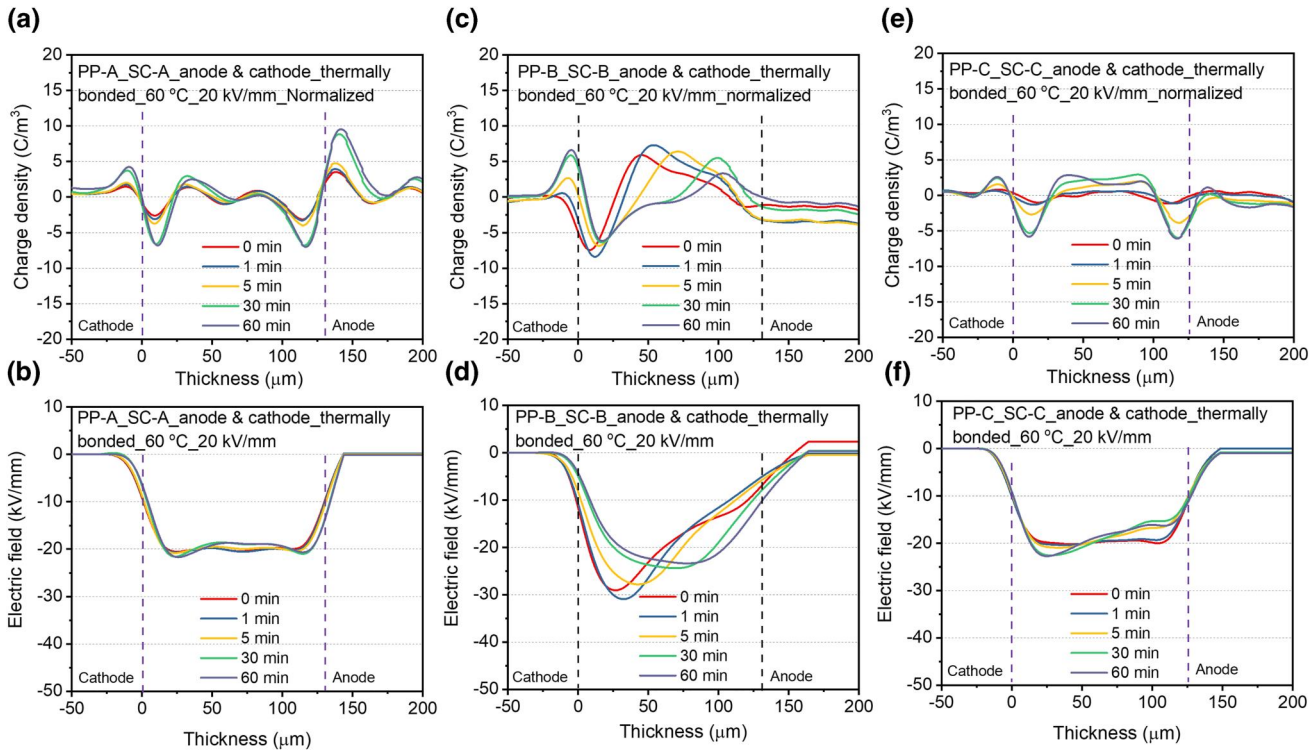

FIGURE 9 Normalised space charge distribution profiles and electric field distortion at DC 20 kV/mm and at 60°C for thermally bonded (a), (b) PP-A; (c), (d) PP-B; (e), (f) PP-C

the anode side with the amplitude of the positive charge peak reduced with time. This was not observed in PP-A at 60°C and 20 kV/mm, indicating higher electric field endowed injected charges higher mobility to transport to the deeper position of the insulation. The dynamism of charge distribution determined the local field distribution. As presented in Figure 10b, the highest local field distortion of 6.0% was found near the anode at 0 min, which decreased and stabilised at 3.2% after 20 min. The enhanced charge mobility and peak shift were also noticed in PP-B. Compared with the PEA data obtained at 60°C and 20 kV/mm, charge distribution measured at 40 kV/mm stabilised after 20 min and reached saturation at a fast speed (Figure 10c). Similar to the data obtained at 20 kV/mm, the maximum field distortion of 23.1% was located near the cathode at 1 min and the value began to decrease and the peak moved to the anode owing to the charge redistribution in the bulk sample. For PP-C, the observed positive charges near the anode (80–100 μm) at 20 kV/mm further moved to the cathode at 40 kV/mm as illustrated in Figure 10e and merged with the positive heterocharge peak near the cathode. Consequently, the electric field near the cathode was severely enhanced by 14.5% (Figure 10f).

Overall, compared with the average charge density measured at 25°C (Figure 8a), higher amount of charges was accumulated in the insulation layer during the voltage-on process at 60°C (Figure 11a), resulting in much higher field distortion (Figure 11c). Among all the three polymer systems, SC-B/PP-B/SC-B experienced the most severe space charge accumulation and insulating property degradation at high temperature, which are due to the weak interface between the two polymer phases. SC-A/PP-A/SC-A slightly outperforms SC-C/PP-C/SC-C at high temperature because of the higher melting temperature of its elastomer phase which ensured higher thermal stability at 60°C. When the voltage was removed, charges in the insulation layer drifted away at a higher speed and less charges were left in the bulk sample at 60°C (Figure 11b) than at 25°C (Figure 8b). Apart from temperature, the applied field also strongly influenced the charge distribution and amount. Intriguingly, the average charge density at 20 kV/mm was even higher than that at 40 kV/mm in PP-A, which might be related to higher charge mobility and more charge recombination that happened at 40 kV/mm. For PP-B and PP-C, the average charge density at 40 kV/mm was higher than 20 kV/mm and these charges were also more mobile.

DC conductivity of thermally bonded sandwich samples was measured at 25°C and 60°C to further validate the effect of temperature on the space charge injection and accumulation. A DC electric field of 40 kV/mm was applied, and the data was recorded for 2 h to obtain the stabilised DC conductivity. At 25°C, the highest DC conductivity was observed in PP-B, followed by PP-C and PP-A (Figure 12). This order is consistent with the maximum field distortion value of these three materials. At 60°C, all samples experienced dramatic increases in their DC conductivity, which support the observation of higher amount of charges with higher mobility in the PEA results. Again, PP-B showed the highest magnitude in DC conductivity. The lowest conductivity was observed in PP-C.

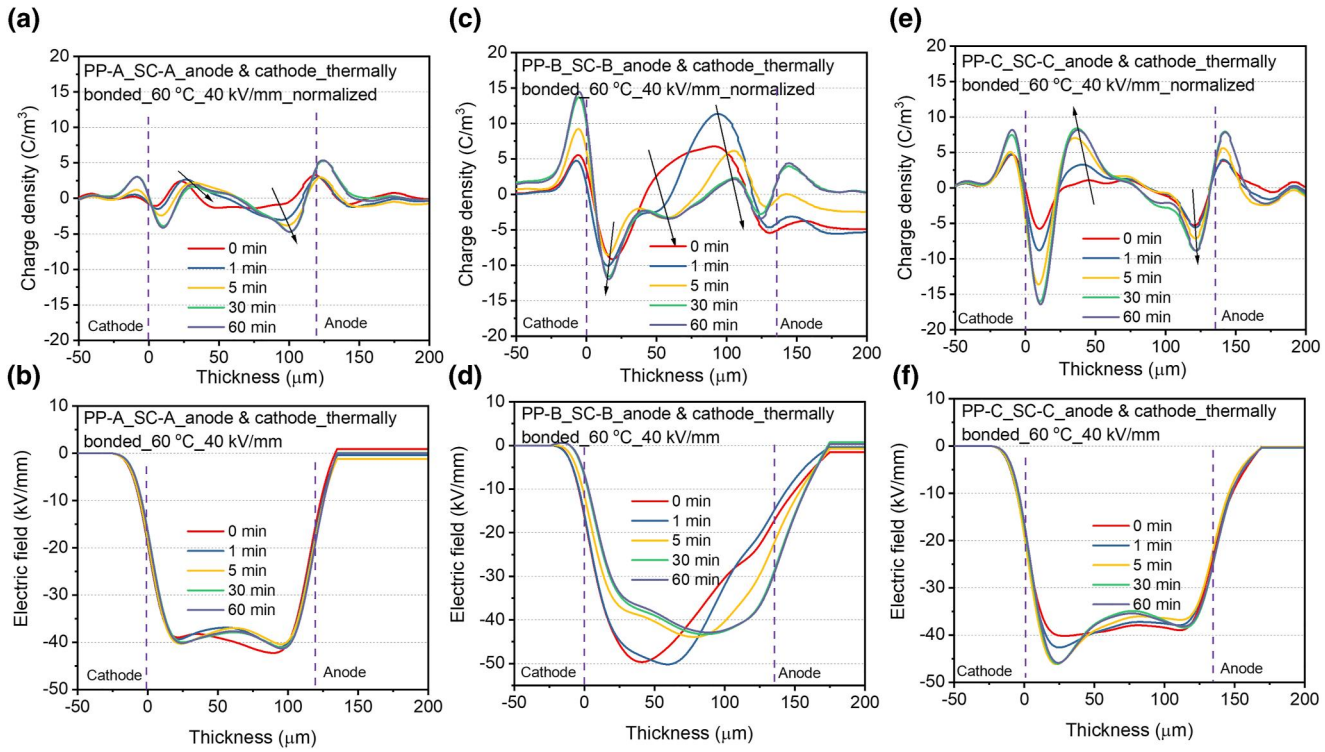

FIGURE 10 Normalised space charge distribution profiles and electric field distortion at DC 40 kV/mm and at 60°C for thermally bonded (a), (b) PP-A; (c), (d) PP-B; (e), (f) PP-C

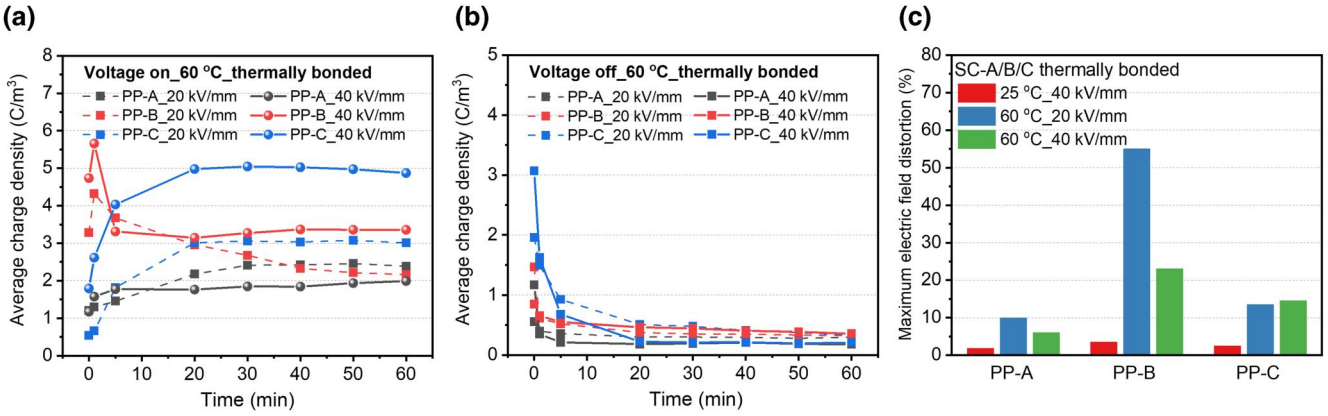

FIGURE 11 Average charge density of thermally bonded SC/PP/SC films at 60°C during (a) voltage-on; (b) voltage off. (c) Comparison of maximum field distortion observed during the voltage-on process of thermally bonded SC/PP/SC films at 25/60°C

4 | CONCLUSIONS

This work presented a detailed investigation on the effect of semiconducting materials on the space charge behaviour of 3 types of PP-based thermoplastic insulating polymers. Mechanically flexible and strong semiconducting materials prepared with 30 wt.% of carbon black showed uniform carbon black nanoparticle dispersion with low electrical resistivity (<5 Ω·cm) over a broad temperature range (25–90°C). Based on the results shown in this work, it was found that the space charge behaviour of the PP-based insulation polymer closely associates with the semiconducting screen attached to it and affected by the bonding method, applied electric field, and temperature. Thermally bonded SC/PP/SC samples demonstrated stronger charge injection than films bonded using natural force. Both homocharge injection from the electrodes and heterocharges accumulation in the sample was significantly enhanced at 60°C compared to 25°C. These injected charges are highly mobile at a high DC field of 40 kV/mm, which potentially migrated from the injection electrode to the opposite electrode and intensified the heterocharge accumulation at the opposite electrode. The higher charge mobility was verified by higher DC conductivity at 60°C. Apart from the charge amount, charge mobility and distribution in the

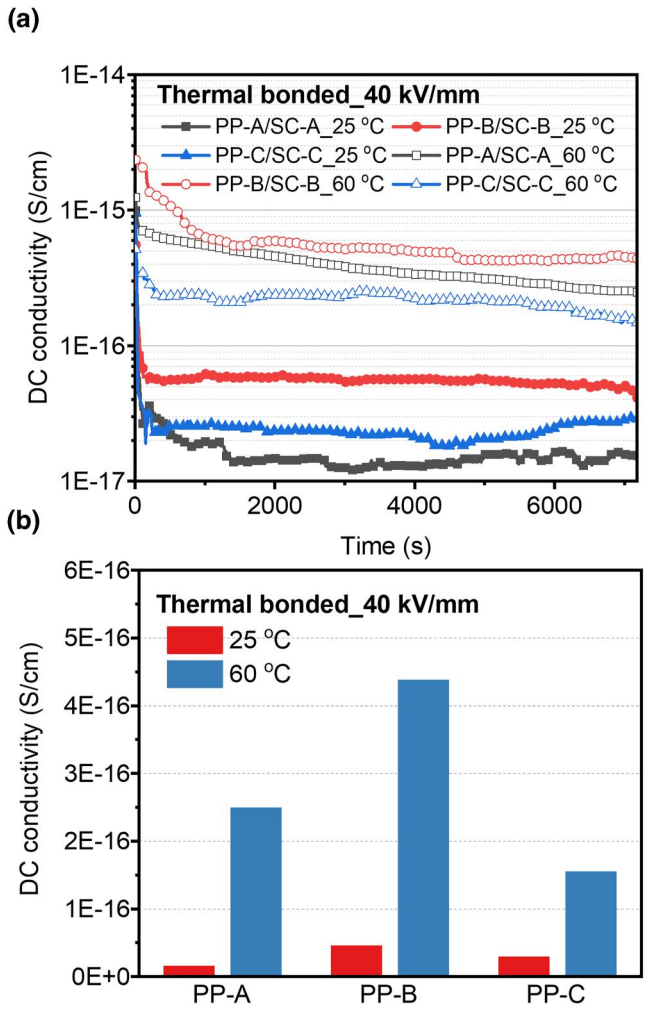

FIGURE 12 Volume electrical resistivity of: (a) SC-A/B/C and a commercial semiconducting material at 25°C; (b) SC-A/B/C as a function of temperature

insulation layer also strongly affected the local electric field distribution. Although thermally bonded PP-B sandwich film exhibited lower amount of accumulated charges at 20 kV/mm and 60°C, the local field which was enhanced was higher than at 40 kV/mm and 60°C due to the higher amount of positive heterocharges near the cathode caused by the lower charge mobility and less charge recombination. Overall, SC-A/C prepared in this work outperforms SC-B and could possibly meet the technical requirement for HVDC cable application. This work highlights the critical role played by semiconducting screens in HVDC cables and provides useful information and guidance on semiconducting screen design for PP-based polymers.

ACKNOWLEDGEMENTS

This work was supported by the Research and Development Program of SGCC in its project entitled 'Research on new generation non-crosslinking extruded MVDC extruded cable technology based on Propylene' (No.5500-201958504A-0-0-00).

DATA AVAILABILITY STATEMENT

The data that support the findings of this study are available from the corresponding author upon reasonable request.

ORCID

Xintong Ren https://orcid.org/0000-0003-2472-4866

REFERENCES

1. Chen, G., et al.: Review of high voltage direct current cables. CSEE J Power Energy Syst. 1(2), 9–21 (2015). https://doi.org/10.17775/cseejpes.2015.00015
2. Fothergill, J.C.: The coming of age of HVDC extruded power cables. IEEE Electrical Insulation Conference (EIC), pp. 124-137. Philadelphia, PA, USA (2014)
3. Mazzanti, G., Marzinotto, M.: Extruded cables for high-voltage direct-current transmission: Advances in research and development. John Wiley & Sons (2013)
4. Du, B., Hou, Z., Li, J.: A review of polypropylene and polypropylene/inorganic nanocomposites for HVDC cable insulation. In: New Trends in High Voltage Engineering (2018). https://doi.org/10.5772/intechopen.80039
5. He, J., Zhou, Y.: Progress in eco-friendly high voltage cable insulation materials. In: 12th International Conference on the Properties and Applications of Dielectric Materials (ICPADM), pp. 11–16. Xi'an, China (2018)
6. Zhou, Y., et al.: Polymeric insulation materials for HVDC cables: Development, challenges and future perspective. IEEE Trans. Dielectr. Electr. Insul. 24(3), 1308–1318 (2017). https://doi.org/10.1109/tdei.2017.006205
7. Hanley, T.L., et al.: A general review of polymeric insulation for use in HVDC cables. IEEE Electr. Insul. Mag. 19(1), 13–24 (2003). https://doi.org/10.1109/mei.2003.1178104
8. Fabiani, D., et al.: Polymeric HVDC cable design and space charge accumulation. Part 1: Insulation/semicon interface. IEEE Electr. Insul. Mag. 23(6), 11–19 (2007). https://doi.org/10.1109/mei.2007.4389975
9. Montanari, G., et al.: Investigating charge trapping properties of combinations of XLPE and semiconductive materials in plaques and cable models. In: International Symposium on Electrical Insulating Materials, pp. 99–102. Kitakyushu, Japan (2005)
10. Nilsson, U.H., Boström, J.: Influence of the semiconductive material on space charge build-up in extruded HVDC cables. IEEE Int. Symp. Electr. Insul., 1–4, San Diego, CA, USA (2010)
11. Hao, M., et al.: The effect of electrode material and semicon bonding on space charge dynamics of XLPE. In: IEEE International Conference on Dielectrics (ICD), pp. 200–203. Montpellier, France (2016)
12. Wei, Y., et al.: Research progress of semiconductive shielding layer of HVDC cable. High Volt. 5(1), 1–6 (2020). https://doi.org/10.1049/hve.2019.0069
13. Niu, F., et al.: Space charge injection in LDPE by semi-conductive electrode with different carbon black filling rates. In: International Symposium on Electrical Insulating Materials, pp. 12–15. KyotoJune, Japan (2014)
14. Huang, X., et al.: Highly conductive polymer nanocomposites for emerging high voltage power cable shields: Experiment, simulation and applications. High Volt. 5(4), 387–396 (2020). https://doi.org/10.1049/hve.2020.0101
15. IEC 60840:2020, Power Cables with Extruded Insulation and Their Accessories for Rated Voltages above 30 kV (Um = 36 kV) up to 150 kV (Um = 170 kV) - Test Methods and Requirements. International Electrotechnical Commission; (2020)
16. IEC 60811-501:2012, Electric and Optical Fibre Cables - Test Methods for Non-metallic Materials - Part 501: Mechanical Tests - Tests for Determining the Mechanical Properties of Insulating and Sheathing Compounds. International Electrotechnical Commission; (2012)
17. Li, W., et al.: Dispersion of carbon blacks and their influence on the properties of semiconductive materials use for high-voltage power cables. In: IEEE International Conference on High Voltage Engineering and

Application (ICHVE), pp. 1–4. Athens, Greece (2018). https://doi.org/10.1109/ichve.2018.8641842
18. Wei, Y., et al.: Charge injection characteristics of semi-conductive composites with carbon black-polymer for HVDC cable. Polymers. 11(7), 1134 (2019). https://doi.org/10.3390/polym11071134
19. Yin, H., et al.: Synthesis of a novel semi-conductive composites doping with La0. 8Sr0. 2MnO3 for excellent electric performance for HVDC cable. Polymers. 12(4), 809 (2020). https://doi.org/10.3390/polym12040809
20. Wang, T., et al.: Influence of charge emission behaviors of semi-conductive shielding layer on charge accumulation properties of insulation layer for HVDC cable. Mater. Res. Express. 7(12), 125302 (2020). https://doi.org/10.1088/2053-1591/abcf7b
21. Xiao, C., et al.: Interface electric field of carbon black loaded electrode and its significant influence on charge injection into polyethylene. J. Appl. Polym. Sci. 123(5), 3017–3022 (2012). https://doi.org/10.1002/app.34950
22. Hao, M., et al.: The impacts of degassing on space charge characteristics and DC conductivity in semicon-bonded XLPE for HVDC cable applications. In: IEEE Conference on Electrical Insulation and Dielectric Phenomena (CEIDP), pp. 97–100. Canada, Toronto (2016)
23. Chong, Y.L., et al.: The effect of degassing on morphology and space charge. In: IEEE International Conference on Solid Dielectrics, vol. 161, pp. 162–165. Toulouse, France (2004)
24. Zha, J.-W., et al.: Morphology and crystalline-phase-dependent electrical insulating properties in tailored polypropylene for HVDC cables. Appl. Phys. Lett. 109(22), 222902 (2016). https://doi.org/10.1063/1.4969063
25. Kurahashi, K., et al.: The application of novel polypropylene to the insulation of electric power cable (3). Electr. Eng. Jpn. 155(3), 1–8 (2006). https://doi.org/10.1002/eej.20114
26. Huang, X., et al.: Polypropylene based thermoplastic polymers for potential recyclable HVDC cable insulation applications. IEEE Trans. Dielectr. Electr. Insul. 24(3), 1446–1456 (2017). https://doi.org/10.1109/tdei.2017.006230
27. Meng, P., et al.: Comparisons of different polypropylene copolymers as potential recyclable HVDC cable insulation materials. IEEE Trans. Dielectr. Electr. Insul. 26(3), 674–680 (2019). https://doi.org/10.1109/tdei.2018.007435
28. Wu, J., Dang, B., Hu, J.: Comparison of effects of ethylene-based and propylene-based copolymer on tailoring the properties of polypropylene. IEEE Access. 8, 123507–123513 (2020). https://doi.org/10.1109/access.2020.3000311
29. Gao, Y., et al.: Compatibility dependent space charge accumulation behavior of polypropylene/elastomer blend for HVDC cable insulation. IEEE Trans. Dielectr. Electr. Insul. 27(3), 947–955 (2020). https://doi.org/10.1109/tdei.2019.008528
30. Gao, Y., et al.: Trap distribution and dielectric breakdown of isotactic polypropylene/propylene based elastomer with improved flexibility for DC cable insulation. IEEE Access. 6, 58645–58661 (2018). https://doi.org/10.1109/access.2018.2874826
31. Smits, F.: Measurement of sheet resistivities with the four-point probe. Bell Syst Tech J. 37(3), 711–718 (1958). https://doi.org/10.1002/j.1538-7305.1958.tb03883.x
32. Liu, N., et al.: Determination of threshold electric field for charge injection in polymeric materials. Appl. Phys. Lett. 106(19), 192901 (2015). https://doi.org/10.1063/1.4921050
33. Zhan, Y., et al.: Space charge measurement and modelling in cross-linked polyethylene. Energies. 13(8), 1906 (2020). https://doi.org/10.3390/en13081906
34. Tang, H., et al.: The positive temperature coefficient phenomenon of vinyl polymer/CB composites. J. Appl. Polym. Sci. 48(10), 1795–1800 (1993). https://doi.org/10.1002/app.1993.070481013
35. Cui, Y., et al.: Effect of ionic conductors on the suppression of PTC and carrier emission of semiconductive composites. Appl. Sci. 10(8), 2915 (2020). https://doi.org/10.3390/app10082915
36. Hao, M., et al.: The impacts of the temperature and electric field on the electrical characteristics in semicon-bonded XLPE insulation.In: IEEE International Conference on High Voltage Engineering and Application (ICHVE), pp. 1–4. Chengdu, China (2016). https://doi.org/10.1109/ichve.2016.7800830

SUPPORTING INFORMATION

Additional supporting information can be found online in the Supporting Information section at the end of this article.

How to cite this article: Zhou, M., et al.: Investigation on effect of semiconducting screen on space charge behaviour of polypropylene-based polymers for HVDC cables. High Volt. 1–14 (2022). https://doi.org/10.1049/hve2.12212